Appl Phys B
DOI 10.1007/s00340-010-4081-z

Applied Physics B
Lasers and Optics

Multifilamentation of high-power femtosecond laser pulse in turbulent atmosphere with aerosol

E.P. Silaeva · S.A. Shlenov · V.P. Kandidov

Received: 18 February 2010 / Revised version: 29 April 2010

Abstract The filamentation of a femtosecond laser pulse in atmosphere under the joint influence of turbulence and aerosol has been numerically studied for the first time. A result of these studies is that the presence of aerosol in a turbulent atmosphere increases the distance to the onset of multifilamentation. We have studied the competition between two factors of aerosol coherent scattering in the process of multiple filamentation of a femtosecond pulse in the atmosphere: generation of light field perturbations and energy losses. Similarity parameters have been determined for different conditions in the problem of multifilamentation in aerosol.

1 Introduction

When femtosecond laser radiation of giga- and terawatt power propagates in atmospheric air, filamentation occurs and laser energy localizes in thin long filaments. The generation of filaments is a result of the dynamic balance between Kerr self-focusing of laser light in air and defocusing in laser-induced plasma that originates in photoionization of the air gaseous components [1–4].

Filamentation of femtosecond laser pulses is accompanied by a number of important effects that find applications in atmospheric optics [5]. Due to the strong nonlinear-optical transformation of the pulse, its spectrum is broadened out and results in a supercontinuum that propagates together with the pulse. The broadband radiation of supercontinuum, for example, is used in femtosecond lidars for remote sensing applications [6]. White light with short duration allows to efficiently probe the composition of atmosphere and to identify pollutants in a wide range of absorption spectra. Femtosecond filaments due to high concentration of laser radiation constitute potential tools for plasma breakdown and generation of fluorescence signal from targets located at distances of several kilometers [7]. Furthermore, plasma channels in filaments can be applied for lightning discharge control [6] and to obtain virtual microwave waveguides [4].

In real conditions, pulses of terawatt power, tens and hundreds times higher than critical power of self-focusing in air, break up into many chaotically located filaments [4, 5]. This results from modulation instability of intense light field in a medium with Kerr nonlinearity [8]. Filaments can be initiated by stochastic perturbations of the light field in the pulse cross-section of the output beam [9] and perturbations caused by the refractive-index fluctuations in turbulent atmosphere [10] and scattering on aerosol particles [11].

Atmospheric turbulence causes fluctuations of air refractive index and thus disturbs phase of the pulse light field. Spatial spectrum of these fluctuations consists of a wide range of scales [10]. Large-scale fluctuations result in random wandering of laser beams as a whole. Small-scale fluctuations influence the processes of filament initiation and formation and lead to random filaments generation in the beam cross-section [40]. In [12], experimental and numerical investigations of single filament wandering on the atmospheric path were performed. Statistical processing of the obtained data showed that filament-center displacements in the transverse plane obey a Rayleigh distribution law. In the more general case of turbulence, the distribution of filaments is better fitted with Weibull distribution law [13]. The typical transversal size of a filament is significantly smaller than the spatial scale of turbulent phase fluctuations. Filament can exist after propagation through a region with strong turbu-

E.P. Silaeva (✉) · S.A. Shlenov · V.P. Kandidov
Faculty of Physics, Lomonosov Moscow State University,
Leninskie gory, Moscow 119991, Russia
e-mail: silaeva@physics.msu.ru
Fax: +7-495-9393091

Published online: 11 June 2010

lence above typical atmospheric values [14]. At the same time, when such region is located on the pulse path before the start of a filament, filament generation probability decreases sharply [13, 15]. Strong turbulence can inhibit the pulse filamentation process.

Filamentation start distance depends strongly on the turbulent conditions on the path. When pulse peak power is slightly greater than the critical power for self-focusing in air, i.e. the regime of a single filament, the distance to filament generation increases with the increase of turbulent fluctuations intensity C_n^2 [16]. When the pulse peak power is high enough and it is possible for multiple filaments to be generated at once, the filament start distance can be either longer or shorter under high values of C_n^2 [17]. In pulses of power P_0 much greater than the critical power P_{cr} for self-focusing in air, turbulent perturbations cause chaotic multiple filamentation and shorten distance to its start [10, 17–20]. Thus, there are two antithetical tendencies in filament formation in turbulent atmosphere. These are the increase of filament start distance under relatively low pulse power and the decrease of this distance, when $P_0 \gg P_{\text{cr}}$ and modulation instability develops. An attempt to quantitatively estimate an interchange between these regimes was performed in [13, 21].

In [10] it is demonstrated that with the growth of the inner scale of atmospheric turbulence l_0, the distance where filaments begin to form increases and the transversal size of filament bunches decreases. In [22] authors show the development of modulation instability in a pulse under turbulence with inner scale values close to those for atmosphere $l_0 = 1$–2 mm. The increase of the inner scale of turbulence up to $l_0 = 6$ mm resulted in suppression of modulation instability development. Besides, small-scale fluctuations of the medium's refractive index can result in the decrease of background coherence, thus preventing energy refill in the filament. According to the opinion of [23], this can lead to the change of typical filaments parameters: their transversal size increases and their peak intensity decreases.

Also, an important factor determining laser filamentation process is the presence of clouds and precipitation on an atmospheric path which results in scattering and attenuation of laser radiation. Laboratory experiments on interaction between filament and single droplets [24] as well as theoretical investigations [25, 26] show that a droplet blocking filament's central core does not inevitably stop its further propagation. Filament is rapidly rebuilt after the droplet.

According to [24, 27], if the density of aerosol particles is high enough ($\sim 10^5$ cm^{-3}), then the energy losses of the formed filament are described by the Bouguer law. Filaments number decrease due to energy losses in aerosol has been registered in a 10 m long fog with droplet density 2.2×10^4 cm^{-3} [28]. Similar results have been obtained in the experiments on filamentation in water when laser pulses propagate through polystyrene suspension [29].

Theoretical investigations of multifilamentation in aerosol usually apply models where droplets are replaced by opaque screens, absorbing light [25, 28], or a scattering medium is replaced by a linear damping medium with an equivalent extinction coefficient [30]. Due to energy losses in aerosol, a filament generates later and its length becomes shorter.

However, under filamentation of laser light in clouds and fogs at the wavelength $\lambda = 800$ nm, for which absorption in water is low, pulse transformation and its energetic characteristics are determined by scattering on aerosol particles [11]. Coherent scattering on particles can initiate multifilamentation and at the same time can cause energy losses [31, 32].

When laser light propagates in turbulent atmosphere with aerosol, the spatial scale of medium inhomogeneities is much greater than the wavelength, the scattering indicatrix is strongly elongated in the forward direction and a significant scattering component remains in the beam. That is why the influence of turbulence and aerosol on filamentation in atmosphere does not result only in energy losses. Laser pulse intensity fluctuations, induced by turbulence and scattering on particles, can stimulate filaments stochastic generation. Filamentation of a high-power femtosecond laser pulse in turbulent atmosphere with aerosol was not currently investigated.

We numerically investigated the influence of aerosol scattering and random phase fluctuations due to turbulence on multifilamentation of a high-power femtosecond laser pulse in atmosphere. We studied the competition of two factors under multifilamentation in the presence of aerosol scattering: light field perturbations generation and energy losses. An average distance to the multifilamentation starting point was determined in different conditions on the path by means of Monte Carlo method. We compared the dynamic scenarios of multiple filaments development, caused by refractive-index random fluctuations, scattering on aerosol particles and their joint influence.

2 Stratified-medium model

Pulse filamentation is considered in the slowly varying envelope approximation. According to it, a stochastic equation for complex amplitude of femtosecond pulse envelope $\widetilde{E}(x, y, z, t)$ in nonlinear randomly inhomogeneous scattering medium is as follows:

$$2ik\frac{\partial \widetilde{E}(x,y,z,t)}{\partial z} = \Delta_\perp \widetilde{E}(x,y,z,t) + \frac{2k^2}{n_0}(\Delta n_{\text{nl}} + \Delta\tilde{n})\widetilde{E}(x,y,z,t) - ik\alpha_{\text{ion}}\widetilde{E}(x,y,z,t) + \widehat{\widetilde{D}}_{\text{aer}}\widetilde{E}(x,y,z,t) \quad (1)$$

where k is the wavenumber, n_0 is the air refractive index, $\widehat{\widetilde{D}}_{\text{aer}}$ stands for the transformation of the light field due to coherent scattering on aerosol particles, $\Delta\tilde{n}(x, y, z)$ is a refractive-index change caused by turbulence. Nonlinear refractive index Δn_{nl} is determined by Kerr nonlinearity Δn_{kerr} and laser-induced plasma Δn_{pl}:

$$\Delta n_{\text{nl}} = \Delta n_{\text{kerr}} + \Delta n_{\text{pl}}. \tag{2}$$

Coefficient α_{ion} describes energy losses caused by multiphoton ionization.

In the model, group velocity dispersion, and therefore space-time focusing, and pulse self-steepening are not taken into account because they are negligible for considered pulse durations (more than 100 fs) and do not affect energetic characteristics studied in these investigations.

Also, in the model we neglect plasma generation inside a water particle. Plasma is generated near shadow surface of a droplet and is significant only for the femtosecond pulse tail [33]. Based on laboratory experiments [34] it was shown that total contribution of free electrons, generated inside aerosol particles, to plasma channels of filaments can be neglected in atmosphere.

For considered pulse duration, it is possible to neglect delayed nonlinear response, caused by induced Raman scattering on rotational transitions of air molecules [35]. Then, the Kerr nonlinear refractive index is instantaneous:

$$\Delta n_{\text{kerr}} = n_2 I, \tag{3}$$

where $I(x, y, z, t) = \frac{c_0 n_0 \varepsilon_0}{2} |\widetilde{E}(x, y, z, t)|^2$ is light intensity, c_0 and n_2 denote light velocity and coefficient of cubic nonlinearity in air, respectively. Since the volume fraction of water in aerosol particles is smaller than 0.001%, its contribution to n_2 value can be neglected. We used $n_2 = 2.4 \times 10^{-19}$ cm^2/W for dry air [2, 4]. This value corresponds to a critical power of self-focusing $P_{\text{cr}} = 4$ GW at the wavelength $\lambda = 800$ nm.

The plasma refractive-index change Δn_{pl} equals:

$$\Delta n_{\text{pl}} = -\frac{e^2 N_e(x, y, z, t)}{2\varepsilon_0 m_e \omega^2}, \tag{4}$$

where m_e and e are electron mass and charge, respectively; ω is light frequency. The electron density $N_e(x, y, z, t)$ is determined according to kinetic equation for photoionization in air [1, 2]:

$$\frac{\partial N_e}{\partial t} = R\big(|E|^2\big)(N_0 - N_e), \tag{5}$$

where ionization rate $R(|E|^2)$ is given by the Perelomov–Popov–Terent'ev model [36], N_0 is the concentration of neutral molecules. For nitrogen N_2 and oxygen O_2, (5) is considered separately, and total electron density N_e is obtained according to their concentration in air.

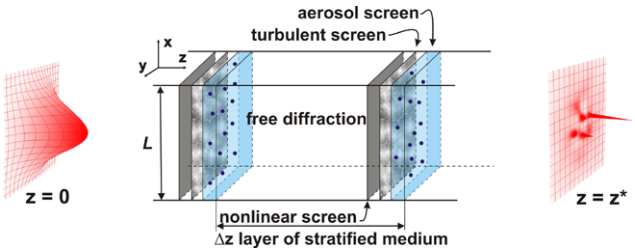

Fig. 1 Stratified-medium model. L is transversal size of the computational area, Δz is the distance between adjacent sets of screens

The extinction coefficient for multiphoton ionization equals:

$$\alpha_{\text{ion}} = \frac{m\hbar\omega}{I(x, y, z, t)} \cdot \frac{\partial N_e(x, y, z, t)}{\partial t}, \tag{6}$$

where m stands for number of photons, necessary to ionize air molecules. For oxygen: $m = 8$, for nitrogen: $m = 10$.

The numerical simulation of the femtosecond laser pulse propagation in atmosphere is based on the stratified-medium model of laser light propagation in nonlinear randomly inhomogeneous scattering media. According to the model, a medium is represented as a sequence of layers with finite thickness Δz (Fig. 1). Every layer is modeled by nonlinear, aerosol and turbulent screens. Free diffraction takes place between the screens. Light field changes, induced by aerosol, turbulence, nonlinearity, dissipation and diffraction in a single layer, are much smaller than the incident on the layer field. At the same time, at the end of propagation path consisting of many stratification layers, field perturbations can be strong. The split-step algorithm along z-coordinate was used to propagate pulse through each layer.

The aerosol screen includes all particles of a layer [37]. It consists of two parallel planes. On the first plane there is an ensemble of spherical particles, where the light field is scattering; on the second plane the light field is determined as a result of interference between waves scattered by droplets and the unperturbed field. Aerosol particles are located randomly in the nodes of a computational grid. The distance between planes of aerosol screen is small to avoid an overlapping of the fields scattered by neighboring particles. For each droplet, scattering is considered in the anomalous diffraction approximation [38]. In order to determine scattering field on the second plane of aerosol screen we calculate the Kirchhoff integral, using a subsidiary computational grid with a step much less than step $\Delta x = \Delta y$ of the main computational grid used to calculate complex amplitude $\widetilde{E}$.

The turbulent screens simulate light field perturbations, caused by refractive-index fluctuations $\Delta\tilde{n}(x, y, z)$ in turbulent atmosphere, described by the modified von Kármán spectrum [39]:

$$F_n(\kappa_x, \kappa_y, \kappa_z) = 0.033 C_n^2 \big(\kappa^2 + \kappa_0^2\big)^{-11/6} \exp\big(-\kappa^2/\kappa_m^2\big), \tag{7}$$

where C_n^2 is the refractive-index structure constant, characterizing the magnitude of turbulent fluctuations; $\kappa_0 = 2\pi/L_0$ and $\kappa_m = 5.92/l_0$, where L_0 and l_0 are outer and inner scales of turbulence, respectively. The two-dimensional spectrum of spatial phase fluctuations on a turbulent screen is as follows [10]:

$$F_\varphi(\kappa_x, \kappa_y) = 2\pi k_0^2 \Delta z F_n(\kappa_x, \kappa_y, 0). \quad (8)$$

The nonlinear screen describes the nonlinear-optical interaction of a pulse with gaseous air components and with laser-induced plasma in a layer.

The problem of diffraction is solved in spectral space for variables (x, y) using Fast Fourier Transform. Equation (5) is integrated over coordinate t using the Euler method for consecutive time slices of the pulse at each step Δz. In the simulations, we used spatially uniform transversal grid with resolution $\Delta x = \Delta y \approx 20$ μm, an adaptive step Δz depending on intensity and nonuniform time grid with minimal step $\Delta t \approx 0.6$ fs increasing to the pulse front and tail. Simulations were performed on two dual-core processors Xeon 2.66 GHz with 16 GB of RAM.

The solution, obtained with a certain sequence of screens, corresponds to the registration of a random field $\widetilde{E}(x, y, z^*, t)$ for a single pulse at given distance z^*. In order to get statistical characteristics of the femtosecond light pulse propagation and filamentation, we used the Monte Carlo method. An ensemble of the fields $\{\widetilde{E}_j(x, y, z^*, t), j = 1, \ldots, M\}$ is obtained as a result of multiple simulations of the pulses propagation in turbulent medium with aerosol, each pulse propagating through a new chain of statistically independent turbulent and aerosol screens.

Scattering on particles and turbulent fluctuations of refractive-index result in wave divergence, and thus some field components quickly deviate away from the propagation direction. In order to avoid field reflection from the edges of the computational grid, an absorption coefficient, smoothly increasing towards the boundary, is introduced. Such absorption removes scattered field from the computational region and thus models energy losses due to scattering.

The problem under consideration is characterized by a wide range of spatial scales:

$$L_0 \gg a_0 \gg l_0 \gg d_{\text{fil}} \gg R_{\text{aer}} \sim h, \quad (9)$$

where d_{fil} stands for the typical filament size.

When analyzing multifilamentation, initiated by turbulent atmosphere and aerosol scattering, we assume that the pulse has Gaussian shape and Gaussian intensity distribution in the cross-section without any field perturbations.

3 Statistical analysis of multifilamentation initiation in aerosol

At first, let us consider influence of just aerosol on high-power femtosecond laser pulse breakup into filaments in atmosphere.

At the initial stage of filamentation when intensity does not reach photoionization threshold $10^{13} \div 10^{14}$ W/cm^2 [41] and plasma is not generated, the power redistribution in the cross-section of the pulse time slices and nonlinear foci formation take place only due to Kerr nonlinearity. That is why filaments initiation in aerosol can be described by (1) at $\Delta n_{\text{pl}} = 0$ and $\alpha_{\text{ion}} = 0$. In case of the absence of turbulence, also $\Delta\tilde{n} = 0$.

In the stationary problem of light self-focusing in aerosol atmosphere, we consider a Gaussian beam, which power P_0 equals to the pulse peak power. The time slice with peak power P_0 self-focuses in a medium with Kerr nonlinearity at the shortest distance, determining the start of a filament. Statistical investigation of multiple filaments initiation has been done by means of the Monte Carlo method for pulses of different power in monodisperse aerosol with particle radius $R_{\text{aer}} = 15$ μm and different concentrations N_{aer}. The results were obtained by averaging of 10 statistically independent realizations of aerosol path.

Figure 2 demonstrates the dependence of the average distance $\langle z_{\text{fil}} \rangle$ to filamentation starting point of the pulse with peak power $P_0 = 400$ GW $(100 P_{\text{cr}})$ on particle concentration N_{aer} in aerosol. Typical intensity distributions $I(x, y)$ of the pulse peak cross-section directly ahead of the first (if any) filament formation are shown in figure insets, illustrating filamentation regimes in the different ranges of particle

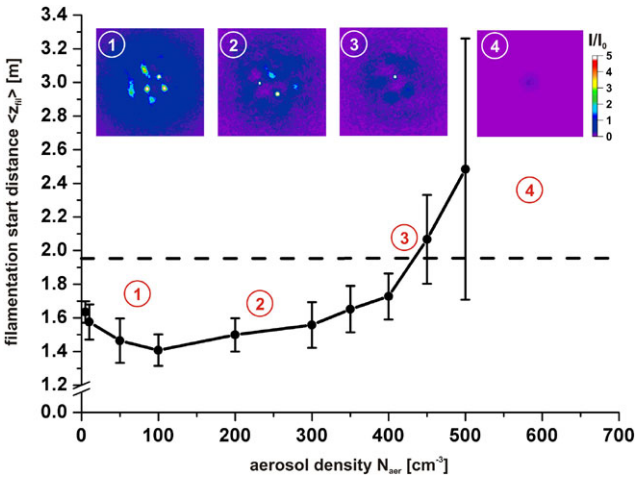

Fig. 2 Dependence of average filamentation distance z_{fil} on aerosol concentration N_{aer} with particle radius $R_{\text{aer}} = 15$ μm for the propagation of the beam with initial parameters: $a_0 = 2.5$ mm, $I_0 = 2 \times 10^{12}$ W/cm^2, $P_0 = 100 P_{\text{cr}}$. *Dashed line* highlights the distance to the starting point of one filament in clear atmosphere. *Numbers in circles* mark different ranges of aerosol concentrations, *insets* showing typical intensity distribution

concentrations. In the range 1 the filamentation start distance decreases with aerosol concentration increase. In this range, the influence of light field perturbations caused by multiple coherent scattering dominates. When concentration increases, there are more sources of interfering scattering patterns and this causes widening of the range of perturbations spatial scales. The probability for perturbations with large growth increment increases, and modulation instability of the intense light field in Kerr medium develops at shorter distance.

With the further increase of particle concentration N_{aer} (range 2), the influence of energy losses due to scattering increases, multiple filaments are initiated at longer distance and their number decreases. At the concentration values from the ranges 1 and 2, pulse power is enough for small-scale self-focusing to occur on the perturbations. This self-focusing occurs before there could be self-focusing of the beam as a whole. Increase of the concentration higher than 430 cm^{-3} (range 3) results in the decrease of intensity level and, thus, in the termination of small-scale self-focusing development. The power in this case is enough only for a single maximum in the vicinity of the beam axis to develop. The distance, where single filament forms, is longer than in clear air. If the concentration value is higher than 500 cm^{-3}, then energy losses caused by aerosol scattering dominate over Kerr self-focusing, and filamentation does not occur.

Filament start distance and particle concentration, at which the change of filaments initiation regimes occurs, depend on initial pulse parameters. So, in a pulse of the same peak power $P_0 = 400$ GW ($100\,P_{\text{cr}}$) but with a larger beam radius $a_0 = 10$ mm, and hence lower peak intensity $I_0 = 1.3 \times 10^{11}$ W/cm^2, filamentation start distance is longer (Fig. 3). Such character of the dependence change is explained in the following way. When intensity decreases, perturbations with the maximal growth increment in Kerr medium [8] has larger spatial scale ($l_{\text{cr}} \sim (P_{\text{cr}}/\pi I_0)^{1/2}$). The growth of spatial scale of perturbations leads to the increase of the distance to their self-focusing, and, therefore the increase of filamentation start distance. At the same time, the range of concentrations N_{aer}, where multifilamentation exists, is shortened, because the influence of energy losses caused by scattering at longer distances also increases.

In order to generalize the obtained results for the different initial parameters of pulse and aerosol medium, we performed a series of simulations where we varied the beam peak power, its radius, the concentration and radius of aerosol particles in a wide range of values, typical for multifilamentation investigations. As a result of statistical analysis, the dependencies of filamentation start distances on particles concentration for the different pulses have been obtained (Fig. 4). For the purpose of generalization we have introduced the following dimensionless variables: filamentation start distance $\zeta_{\text{fil}} = z_{\text{fil}}/kl_{\text{cr}}^2$, normalized to diffraction length of a perturbation containing critical power for self-focusing and medium optical thickness $\tau_{\text{aer}} = 2\pi R_{\text{aer}}^2 N_{\text{aer}} z_{\text{fil}}^*$, where z_{fil}^* is the minimal distance of multifilamentation. For example, in the case, presented in Fig. 2, this distance is $z_{\text{fil}}^* = 1.4$ m and in Fig. 3 it is $z_{\text{fil}}^* = 27$ m. In these dimensionless variables, the obtained dependencies are close to each other (Fig. 4). When particle concentration is low and optical thickness at the filamenta-

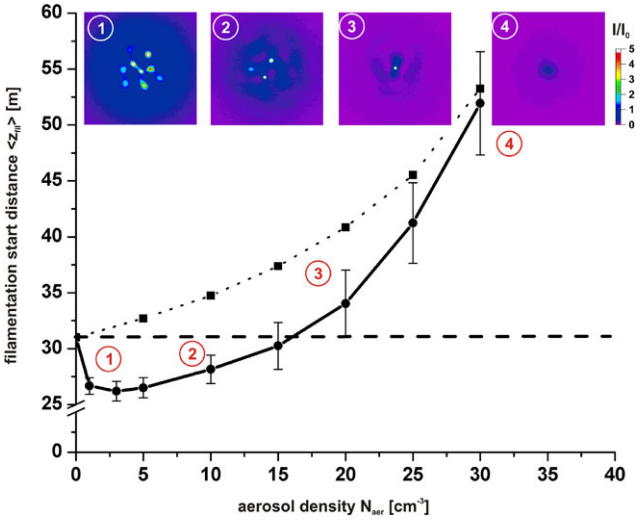

Fig. 3 Dependence of filamentation distance z_{fil} on aerosol concentration N_{aer} with particle radius $R_{\text{aer}} = 15$ μm for the beam with initial parameters: $a_0 = 10$ mm, $I_0 = 1.3 \times 10^{11}$ W/cm^2, $P_0 = 100 P_{\text{cr}}$ in aerosol medium (*solid curve*) and in linear damping medium with the extinction coefficient $\alpha_0 = 2\pi R_{\text{aer}}^2 N_{\text{aer}}$ (*dotted curve*). *Dashed line* highlights the distance to the starting point of one filament in clear atmosphere. *Numbers in circles* mark different ranges of aerosol concentrations, *insets* showing typical intensity distribution

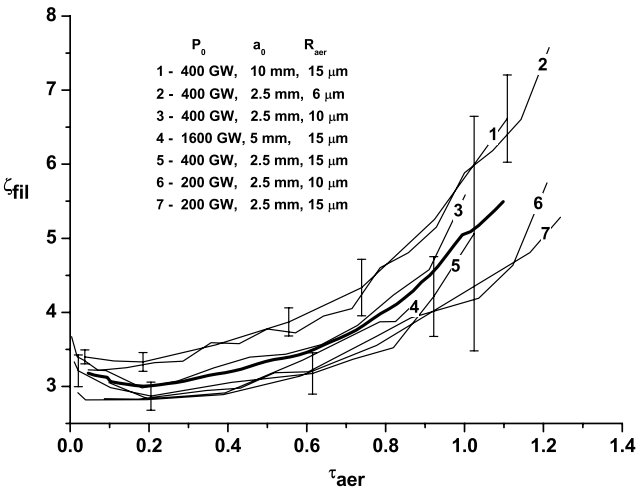

Fig. 4 Dependence of filamentation start distance on aerosol optical thickness for different pulses and different radii of aerosol particles, expressed in terms of dimensionless variables: $\zeta_{\text{fil}} = z_{\text{fil}}/kl_{\text{cr}}^2$ and $\tau_{\text{aer}} = 2\pi R_{\text{aer}}^2 N_{\text{aer}} z_{\text{fil}}^*$. *Bold curve* is the generalization of the depicted results

Table 1 Filamentation start distance, m

Pulse ($P_0 = 400$ GW)	a_0, cm	1	1	2
Turbulence parameters	C_n^2, cm$^{-2/3}$	10^{-16}	10^{-16}	10^{-17}
($L_0 = 1$ m, $l_0 = 1$ mm)	$d_{\text{ext}}^{\text{turb}}$, m	2300	2300	8400
Aerosol parameters	R_{aer}, μm	15	15	5
	N_{aer}, cm^{-3}	10	25	10
	$d_{\text{ext}}^{\text{aer}}$, m	71	29	637
Turbulent transparent medium	$\tilde{z}_{\text{turb}}$	24.6	24.6	97.4
Aerosol without turbulence	$\langle z_{\text{aer}} \rangle$	28.0 ± 1.4	41.2 ± 3.6	104.3 ± 6.1
Turbulent medium with aerosol	$\langle z_{\text{turb+aer}} \rangle$	27.2 ± 1.1	41.1 ± 3.9	100.1 ± 5.0
Turbulent medium with linear damping		29.4	44.5	104.2

tion start distance is $\tau_{\text{aer}} < 0.2$, influence of the light field perturbations determines multifilamentation. When particle concentration is high and optical thickness at the filamentation start distance is $\tau_{\text{aer}} > 0.2$, energy losses are crucial.

It is of practical interest to estimate if it is possible to replace the scattering aerosol by an equivalent linear damping medium in the filamentation study. The extinction coefficient α_0 is determined by aerosol parameters:

$$\alpha_0 = 2\pi N_{\text{aer}} R_{\text{aer}}^2. \tag{10}$$

In Fig. 3, the dotted line shows the dependence of filamentation start distance on concentration value, determining the extinction coefficient α_0 of linear damping medium. In this medium, only one filament forms at any particle concentration and at a distance longer than in clear air. Only one filament forms also in a stochastic aerosol medium (solid curve in Fig. 3) with concentration from the range 3, however its generation begins at a shorter distance. Because, in spite of the predominance of energy losses, the initial field perturbations caused by scattering on particles serve as a seed for filament formation. Only for high concentration the results of statistical analysis and deterministic approach on the basis of linear damping medium model agree within confidence limits. These results correspond qualitatively to the results of the work in [28].

4 Filamentation in turbulent atmosphere with aerosol

Using a stationary approximation, we have statistically analyzed the influence of aerosol scattering on the distance to multifilamentation start of the pulse in turbulent atmosphere. We considered laser beam with radius $a_0 = 10$ mm and initial peak power $P_0 = 400$ GW, corresponding to intensity $I_0 = 1.3 \times 10^{11}$ W/cm^2.

In aerosol ($N_{\text{aer}} = 10$ cm^{-3}, $R_{\text{aer}} = 15$ μm, $\alpha_0 = 0.014$ m^{-1}) in the absence of turbulence an average distance to filamentation start for such pulse is $\langle z_{\text{aer}} \rangle = 28.0 \pm 1.4$ m (Table 1). For a certain realization of refractive-index fluctuations $\tilde{n}(x, y, z)$ on the path in turbulent transparent atmosphere ($C_n^2 = 10^{-16}$ cm$^{-2/3}$, $L_0 = 1$ m, $l_0 = 1$ mm) multifilamentation starts at a closer distance $\tilde{z}_{\text{turb}} = 24.6$ m. On the same turbulent path with the same fluctuations $\tilde{n}(x, y, z)$, the presence of the aforementioned aerosol leads to the increase of the average filamentation start distance $\langle z_{\text{turb+aer}} \rangle = 27.2 \pm 1.1$ m. In order to find the cause of distance increase due to aerosol scattering, we have studied pulse filamentation at the same turbulence in linear damping medium with the same extinction coefficient as in the aerosol. It turned out that under these conditions the filamentation start distance is longer than in turbulent aerosol atmosphere and equals 29.4 m. This means that in a turbulent atmosphere, aerosol scattering slows down multifilamentation due to pulse energy losses, while in contrast, it stimulates filament initiation on the field perturbations caused by coherent scattering. This conclusion is confirmed by the results, obtained in simulations with different parameters of the turbulent aerosol medium and the pulse (Table 1).

We considered a possibility to use extinction length for analysis of multifilamentation of laser light in atmosphere. When light propagates in a turbulent atmosphere, the intensity decreases due to turbulent broadening of the beam on average. In a Gaussian approximation, the turbulent change of the average intensity with distance is described by [39]:

$$I(r, z) = \frac{I_0}{(1 + 1.63\sigma_1^{12/5}\Lambda)} \times \exp\left(-\frac{r^2}{a_0(1 + 1.63\sigma_1^{12/5}\Lambda)}\right) \tag{11}$$

where $\sigma_1^2 = 1.23 C_n^2 k^{7/6} z^{11/6}$ is the Rytov variance of intensity fluctuations associated with a plane wave, $\Lambda = z/ka_0^2$ is the distance in diffraction lengths. In this approximation the typical extinction length in turbulence $d_{\text{ext}}^{\text{turb}}$ is about 1000 m and much higher than in aerosol $d_{\text{ext}}^{\text{aer}} = 1/\alpha_0$ (see (10)) which is typically 10–100 m, whereas the distances to

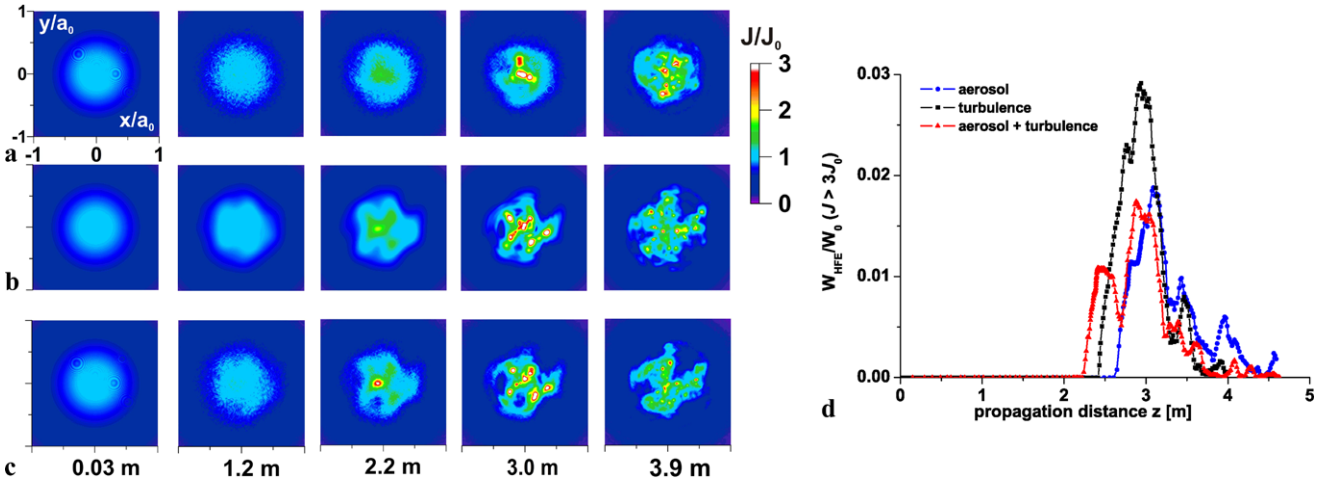

Fig. 5 Fluence distribution $J/J_0(x, y)$ at different distances z (**a**), (**b**), (**c**) and relative high-fluence energy W_{HFE}/W_0 $(J > 3J_0)$ dependence on distance (**d**) of the pulse (**a**) in aerosol with concentration $N_{\mathrm{aer}} = 10\ \mathrm{cm}^{-3}$ and particles radius $R_{\mathrm{aer}} = 15\ \mu\mathrm{m}$, (**b**) in turbulent atmosphere with parameters: structure constant $C_n^2 = 10^{-13}\ \mathrm{cm}^{-2/3}$, inner scale $l_0 = 1$ mm, outer scale $L_0 = 1$ m, (**c**) in turbulent atmosphere with aerosol, medium parameters are the same as in (**a**) and (**b**). Pulse parameters: duration $\tau_p = 280$ fs, radius $a_0 = 2.5$ mm, initial peak intensity $I_0 = 10^{12}\ \mathrm{W/cm}^2$, initial peak fluence $J_0 = 0.25\ \mathrm{J/cm}^2$, $W_0 = 50$ mJ

the filamentation onset in both cases are of the same order of magnitude (Table 1). Thus, the extinction length is not a similarity criterion for the problem of femtosecond pulse multifilamentation in atmosphere.

5 Dynamic scenario of multifilamentation in atmosphere

We considered a dynamic problem of multifilamentation in atmosphere in order to compare the influence of turbulence and aerosol on filaments development along the propagation path. A stochastic breakup of a pulse at a random distribution of aerosol particles and refractive-index fluctuations in atmosphere is described by (1)–(8). Preliminary analysis shows that a demonstrative dynamic scenario of pulse multifilamentation takes place in low density aerosol with large droplets. We considered aerosol with $R_{\mathrm{aer}} = 15\ \mu\mathrm{m}$ and $N_{\mathrm{aer}} = 10\ \mathrm{cm}^{-3}$ and strong turbulence with $C_n^2 = 10^{-13}\ \mathrm{cm}^{-2/3}$ [39] and $l_0 = 1$ mm, $L_0 = 1$ m.

Laser pulse parameters were as follows: wavelength $\lambda = 800$ nm, duration $\tau_p = 280$ fs (e^{-1} intensity level), energy 50 mJ and beam radius $a_0 = 2.5$ mm (e^{-1} intensity level). At these parameters, peak fluence is $J_0 = 0.25\ \mathrm{J/cm}^2$ and peak power is $P_0 = 200$ GW, it corresponds to $P_0 = 50P_{\mathrm{cr}}$. The duration of the pulse, slightly longer than usually used in experiments, allows to safely neglect group velocity dispersion and delayed Kerr response in the model.

Under such parameters of the pulse and atmosphere multifilamentation develops approximately at the same distance for the given pulse propagation in aerosol and turbulence separately (Figs. 5(a), (b)). The maximum value of fluence, achieved in these numerical simulations, is $10J_0$.

Both stochastic factors in atmosphere, aerosol and turbulence, result in the formation of the light field perturbations in the pulse cross-section, which cause multifilamentation. However, these perturbations are different by nature: amplitude perturbations due to the interference of scattering patterns in aerosol and phase field perturbations in turbulent atmosphere form essentially different fluence distributions $J(x, y)$ at the same distances (Figs. 5(a), (b)). In the early beginning of the aerosol path, there are visible small-scale perturbations in the fluence distribution in the form of diffraction rings due to scattering on the separate droplets. Slightly further, the fluence distribution of the pulse propagating in pure aerosol is manifested as a speckle pattern. However filament initiation occurs at a significantly longer distance. The perturbations, induced by turbulence, have larger scale and become visible in the fluence distribution only at a distance close to the filamentation start. The number of filaments in turbulence is more than in aerosol atmosphere.

In turbulent aerosol medium, small-scale perturbations in aerosol superpose on large-scale turbulent perturbations. At the beginning of the path, turbulence dominates and determines the initial location of the "hot" spots in fluence distribution (Fig. 5(c)). However, later on the interplay between scattering on aerosol particles and refractive-index fluctuations leads to energy redistribution in the pulse and "hot" spot displacements in comparison to the case of transparent turbulent atmosphere (Fig. 5(b)).

Pulse energy losses in these media are also different. We considered the amount of energy localized by filament,

namely energy where fluence is high (high-fluence energy HFE), for example, with $J > 3J_0$. Figure 5(d) shows that HFE in aerosol is less than in turbulent medium and energy losses, caused by aerosol scattering, dominate in HFE change with distance in atmosphere with both turbulence and aerosol.

6 Conclusions

We have studied numerically in the process of femtosecond laser pulse multifilamentation the competition between two factors, related to aerosol scattering: generation of light field perturbations and energy losses. Dimensionless variables in the problem of multifilamentation in aerosol are the filamentation start distance, normalized to diffraction length of a scale containing critical power for self-focusing, and medium optical thickness at the minimal distance of multifilamentation starting point. We showed that, when a pulse propagates in atmospheric aerosol with small optical thickness ($\tau_{aer} < 0.2$) at a typical filamentation start distance, the influence of perturbations caused by coherent scattering dominate and multifilamentation develops. With the increase of optical thickness ($\tau_{aer} > 0.2$), pulse energy losses caused by scattering becomes substantial and filamentation start distance increases, number of filaments decreasing. Further growth of optical thickness results in the regime of a single filament and, finally, filamentation suppression.

The filamentation of a high-power femtosecond laser pulse in the joint influence of turbulence and aerosol scattering has been investigated for the first time. We have determined that the presence of aerosol in turbulent atmosphere increases distance to filamentation start.

The replacement of an aerosol medium by a linear damping medium with the same extinction coefficient applies only when the energy losses caused by scattering dominate during filamentation process.

Acknowledgements This work has been funded by the Russian Federal Agency for Science and Innovations (Rosnauka) under the state contract 02.740.11.0223.

References

1. S.L. Chin, S.A. Hosseini, W. Liu, Q. Luo, F. Berge, N. Akozbek, A. Becker, V.P. Kandidov, O.G. Kosareva, H. Schroeder, Can. J. Phys. **83**, 863 (2005)
2. A. Couairon, A. Mysyrowicz, Phys. Rep. **441**, 41 (2007)
3. L. Berge, S. Skupin, R. Nuter, J. Kasparian, J.P. Wolf, Rep. Prog. Phys. **70**, 1633 (2007)
4. V.P. Kandidov, S.A. Shlenov, O.G. Kosareva, Quantum Electron. **39**, 205 (2009)
5. J. Kasparian, J.-P. Wolf, Opt. Express **16**, 466 (2008)
6. J. Kasparian, M. Rodriguez, G. Mejean, J. Yu, E. Salmon, H. Wille, R. Bourayou, S. Frey, Y.-B. Andre, A. Mysyrowicz, R. Sauerbrey, J.-P. Wolf, L. Woste, Science **301**, 61 (2003)
7. S.L. Chin, H.L. Xu, Q. Luo, F. Théberge, W. Liu, J.F. Daigle, Y. Kamali, P.T. Simard, J. Bernhardt, S.A. Hosseini, M. Sharifi, G. Méjean, A. Azarm, C. Marceau, O. Kosareva, V.P. Kandidov, N. Aközbek, A. Becker, G. Roy, P. Mathieu, J.R. Simard, M. Châteauneuf, J. Dubois, Appl. Phys. B Lasers Opt. **95**, 1 (2009)
8. V.I. Bespalov, V.I. Talanov, JETP Lett. **3**, 307 (1966)
9. S. Skupin, L. Bergé, U. Peschel, F. Lederer, G. Méjean, J. Yu, J. Kasparian, E. Salmon, J.P. Wolf, M. Rodriguez, L. Wöste, R. Bourayou, R. Sauerbrey, Phys. Rev. E Stat. Nonlinear Soft Matter Phys. **70**, 046602 (2004)
10. S.A. Shlenov, V.P. Kandidov, Atmos. Ocean. Opt. **17**, 637 (2004)
11. V.O. Militsin, E.P. Kachan, V.P. Kandidov, Quantum Electron. **36**, 1032 (2006)
12. S.L. Chin, A. Talebpour, J. Yang, S. Petit, V.P. Kandidov, O.G. Kosareva, M.P. Tamarov, Appl. Phys. B Lasers Opt. **74**, 67 (2002)
13. A. Houard, M. Franco, B. Prade, A. Durécu, L. Lombard, P. Bourdon, O. Vasseur, B. Fleury, C. Robert, V. Michau, A. Couairon, A. Mysyrowicz, Phys. Rev. A At. Mol. Opt. Phys. **78**, 033804 (2008)
14. R. Salamé, N. Lascoux, E. Salmon, R. Ackermann, J. Kasparian, J.P. Wolf, Appl. Phys. Lett. **91**, 171106 (2007)
15. R. Ackermann, G. Méjean, J. Kasparian, J. Yu, E. Salmon, J.P. Wolf, Opt. Lett. **31**, 86 (2006)
16. J.R. Penano, P. Sprangle, B. Hafizi, A. Ting, D.F. Gordon, C.A. Kapetanakos, Phys. Plasmas **11**, 2865 (2004)
17. S.A. Shlenov, V.P. Kandidov, O.G. Kosareva, A.E. Bezborodov, V.Y. Fedorov, Proc. SPIE **6733**, 67332M (2007)
18. V.P. Kandidov, O.G. Kosareva, M.P. Tamarov, A. Brodeur, S.L. Chin, Quantum Electron. **29**, 911 (1999)
19. S.A. Shlenov, A.I. Markov, Quantum Electron. **39**, 658 (2009)
20. G. Paunescu, G. Spindler, W. Riede, H. Schröder, A. Giesen, Appl. Phys. B Lasers Opt. **96**, 175 (2009)
21. G. Fibich, S. Eisenmann, B. Ilan, Y. Erlich, M. Fraenkel, Z. Henis, A.L. Gaeta, A. Zigler, Opt. Express **13**, 5897 (2005)
22. G. Spindler, G. Paunescu, Appl. Phys. B Lasers Opt. **96**, 185 (2009)
23. Y.-Y. Ma, X. Lu, T.-T. Xi, Q.-H. Gong, J. Zhang, Opt. Express **16**, 8332 (2008)
24. F. Courvoisier, V. Boutou, J. Kasparian, E. Salmon, G. Mejean, J. Yu, J.-P. Wolf, Appl. Phys. Lett. **83**, 213 (2003)
25. M. Kolesik, J.V. Moloney, Opt. Lett. **29**, 590 (2004)
26. S. Skupin, L. Berge, U. Peschel, F. Lederer, Phys. Rev. Lett. **93**, 023901 (2004)
27. N.N. Bochkarev, A.A. Zemlyanov, A.A. Zemlyanov, A.M. Kabanov, D.V. Kartashov, A.V. Kirsanov, G.G. Matvienko, A.N. Stepanov, Atmos. Ocean. Opt. **17**, 971 (2004)
28. G. Mejean, J. Kasparian, J. Yu, E. Salmon, S. Frey, J.-P. Wolf, S. Skupin, A. Vinaotte, R. Nuter, S. Champeaux, L. Berge, Phys. Rev. E, Stat. Nonlinear Soft Matter Phys. **72**, 026611 (2005)
29. V. Jukna, G. Tamošauskas, G. Valiulis, M. Aputis, M. Puida, F. Ivanauskas, A. Dubietis, Appl. Phys. B Lasers Opt. **94**, 175 (2009)
30. A.A. Zemlyanov, Y.E. Geints, Opt. Commun. **259**, 799 (2006)
31. E.P. Silaeva, V.P. Kandidov, Atmos. Ocean. Opt. **22**, 26 (2009)
32. V.P. Kandidov, E.P. Silaeva, J. Russ. Laser Res. **30**, 305 (2009)
33. V.P. Kandidov, O.V. Militsin, Atmos. Ocean. Opt. **17**, 54 (2004)
34. S. Henin, Y. Petit, D. Kiselev, J. Kasparian, J.P. Wolf, Appl. Phys. Lett. **95**, 091107 (2009)
35. K.Y. Andrianov, V.P. Kandidov, O.G. Kosareva, S.L. Chin, A. Talebpur, S. Petit, W. Liu, A. Ivasaki, M.C. Nadeau, Izv. Akad. Nauk Ser. Fiz. **66**, 1091 (2002)
36. A.M. Perelomov, V.S. Popov, M.V. Terent'ev, Sov. Phys. JETP **23**, 924 (1966)
37. V.O. Militsin, L.S. Kuzminsky, V.P. Kandidov, Atmos. Ocean. Opt. **18**, 789 (2005)

38. H.C. Van de Hulst, *Light Scattering by Small Particles* (Dover, New York, 1981)
39. L.C. Andrews, R.L. Phillips, *Laser Beam Propagation Through Random Media* (SPIE, Bellingham, 1998)
40. S.A. Shlenov, V.P. Kandidov, Atmos. Ocean. Opt. **17**, 630 (2004)
41. J. Kasparian, R. Sauerbrey, S.L. Chin, Appl. Phys. B Lasers Opt. **71**, 877 (2000)